

# REPORT DOCUMENTATION PAGE

Form Approved OMB No. 0704-0188

Public reporting burden for this collection of information is estimated to average 1 hour per response, including the time for reviewing instructions, searching existing data sources, gathering and maintaining the data needed, and completing and reviewing the collection of information. Send comments regarding this burden estimate or any other aspect of this collection of information, including suggestions for reducing this burden to Washington Headquarters Services, Directorate for Information Operations and Reports, 1215 Jefferson Davis Highway, Suite 1204, Arlington, VA 22202-4302, and to the Office of Management and Budget, Paperwork Reduction Project (0704-0188), Washington, DC 20503.

1. AGENCY USE ONLY (Leave blank)		2. REPORT DATE 26 January 2005	3. REPORT TYPE AND DATES COVERED Final Report, 16 December 2003 to 16 December 2004	
4. TITLE AND SUBTITLE An Investigation of Certain Thermodynamic Losses in Minature Cryocoolers			5. FUNDING NUMBERS	
6. AUTHOR(S) Dr. Jaime Reed				
7. PERFORMING ORGANIZATION NAME(S) AND ADDRESS(ES) University of Oxford Parks Road Oxford OX1 3PJ United Kingdom			8. Performing Organization Report Number	
9. SPONSORING/MONITORING AGENCY NAME(S) AND ADDRESS(ES) EOARD PSC 802 Box 14 FPO 09499-0014			10. SPONSORING/MONITORING AGENCY REPORT NUMBER SPC 04-3011	
11. SUPPLEMENTARY NOTES 29 pages. Person responsible: Barrett A. Flake, telephone number +44 (0)20 7514 4285.				
12a. DISTRIBUTION/AVAILABILITY STATEMENT Approved for public release; distribution is unlimited.			12b. DISTRIBUTION CODE A	
ABSTRACT (Maximum 200 words)  Stirling cycle cryocoolers developed at Oxford have typically been designed using a second order methods whereby the ideal Stirling efficiency is degraded by a number of discrete loss mechanisms. In all cases the eventual machines perform less well than expected, and it always appears as if an additional thermodynamic loss is acting. This empirically calibrated loss is therefore included as part of the normal design procedure and there is anecdotal evidence that this is an approach taken by other manufactures. Although this loss might be caused by imperfect heat transfer, existing theories do not agree with its magnitude. A project was therefore started to measure the losses in the simplest possible geometry, a linear compressor with a plain 'top-hat' cylinder head. It was hoped that by characterizing the losses in this geometry and applying them to full machines these called "compression loss" could be explained. Since the loss is quite large it could allow significant improvements to be made for future machines. A well calibrated measurement system was developed and a linear compressor commissioned. To enable a sufficiently good energy balance to be produced electromagnetic motor losses and windage were measured. It immediately became clear that these were more significant than had been assumed previous studies. In fact it appeared as if a significant proportion of the "compression loss" might be explained by these new measurements. With the losses expected from analytic analyses. Agreement was not perfect, however, and this is thought to be due to the incompleteness of the heat transfer theory, particularly with regard to the flow through the clearance seal. Future possibilities for work are suggested and it is hoped that these measurements can be used as a baseline for testing theoretical work which will enable efficiencies to be increased not just in Stirling type coolers, but also in pulse tubes and linear alternators.				
14. SUBJECT TERMS EOARD, Stirling, Compressor, Losses, Cryocoolers, Thermodynamics			15. NUMBER OF PAGES	
			16. PRICE CODE	
17. SECURITY CLASSIFICATION OF REPORT UNCLASSIFIED	18. SECURITY CLASSIFICATION OF THIS PAGE UNCLASSIFIED	19. SECURITY CLASSIFICATION OF ABSTRACT UNCLASSIFIED	20. LIMITATION OF ABSTRACT UL	



# AN INVESTIGATION OF CERTAIN THERMODYNAMIC LOSSES IN MINIATURE CRYOCOOLERS

## *FINAL REPORT*

---

AUTHOR: Jaime Reed, Cryogenics Group, Oxford University

REPORT FOR: USAF EOARD  
DATE: 17/JAN/2005  
NUMBER OF PAGES: 29

CONTRACT: FA8655-04-1-3011  
ADDITIONAL DOCUMENTS: NONE.  
OUR REF: LOS-FR1

---

## Contents

Executive summary .....	3
1. Background .....	4
2. Introduction .....	4
3. Instrumentation.....	5
4. Energy balance in the compressor .....	10
5. Preliminary tests .....	12
6. Comparison of windage/motor losses to compression loss measurements in original cooler configuration .....	18
7. Compression measurements .....	19
8. Conclusions .....	21
References .....	23
Table of notation.....	24
Appendix A. Expressions used to calculate the losses .....	25

## **Executive summary**

Stirling cycle cryocoolers developed at Oxford have typically been designed using a second order method whereby the ideal Stirling efficiency is degraded by a number of discrete loss mechanisms. In all cases the eventual machines perform less well than expected, and it always appears as if an additional thermodynamic loss is acting. This empirically calibrated loss is therefore included as part of the normal design procedure and there is anecdotal evidence that this is an approach taken by other manufacturers. Although this loss might be caused by imperfect heat transfer, existing theories do not agree with its magnitude. A project was therefore started to measure the losses in the simplest possible geometry, a linear compressor with a plain 'top-hat' cylinder head. It was hoped that by characterizing the losses in this geometry and applying them to full machines these called "compression loss" could be explained. Since the loss is quite large it could allow significant improvements to be made for future machines.

A well calibrated measurement system was developed and a linear compressor commissioned. To enable a sufficiently good energy balance to be produced electromagnetic motor losses and windage were measured. It immediately became clear that these were more significant than had been assumed in previous studies. In fact it appeared as if a significant proportion of the "compression loss" might be explained by these new measurements.

With the new motor loss measurements the thermodynamic losses were measured and found to agree much better with the clearance seal and heat transfer losses expected from analytic analyses. Agreement was not perfect, however, and this is thought to be due to the incompleteness of the heat transfer theory, particularly with regard to the flow through the clearance seal.

Future possibilities for work are suggested and it is hoped that these measurements can be used as a baseline for testing theoretical work which will enable efficiencies to be increased not just in Stirling type coolers, but also in pulse tubes and linear alternators.

## 1. Background

A Stirling cycle cryocooler can be considered as undergoing an ideal cycle (with Carnot efficiency), with loss processes degrading the performance (a so called 'second-order' analysis). We have quantified these losses by means of an energy balance analysis in several machines [1,2]. The input power and individual loss processes were all measured and an excellent energy balance was obtained, which led us to believe that we had accounted for all the processes of any significance. In all cases a significant proportion of the power delivered to the gas (45% in one case), was accounted for by one process which was proportional to frequency, swept volume, and peak-to-peak pressure. We measured this loss in a number of different cryocoolers and over a wide range of variables. It therefore appeared to be some thermodynamic cycle which was quite independent of the refrigeration cycle, taking place in the ambient temperature part of the system as a result of cyclic pressure changes.

One mechanism which had not been accounted for was imperfect heat exchange between the gas and cylinder walls. Several theoretical and empirical correlations have been produced for this but none could fully explain the loss. Although we have no detailed understanding of this thermodynamic process, we did produce an empirical correlation which was incorporated into a computer based model for Stirling cycle coolers. This very successfully predicted cooler performance over a wide range of cooler size and operating temperatures from 60 K to 300 K. Although the loss can only be directly measured in split Stirling cycle machines, due to the ability to hold the displacer stationary, it is likely to also occur in both pulse tube machines and linear alternators, due the similar geometries. The loss is large enough that a small reduction in its value would produce a significant improvement in cryocooler efficiency. The current project has been focused on developing reliable and accurate methods of measuring the loss processes in a compressor operating at ambient temperatures. Without the addition of an obvious load, such as a pulse tube, it should be possible to measure the intrinsic losses in compressors and better understand their operation.

## 2. Introduction

Measurement of the losses in a Stirling cycle cryocooler is not trivial as they are numerous and interdependent. They can be represented, however, in a simplified form as shown in figure 1. If the displacer is held stationary then no cooling work is done and only the ambient temperature losses occur. In this case the cryocooler is equivalent to a compressor and therefore these losses can be investigated by a plain geometry without the need for a regenerator or cold-finger.

To achieve this simplified geometry an existing cryocooler, developed for a domestic refrigerator [2], was disassembled and the compressor removed as shown in figure 2. This was of the conventional moving coil design, the piston diameter was 18 mm and the maximum peak-to-peak stroke was 17.52 mm, giving a maximum peak-to-peak swept volume of 4.46 cc. The compressor was mounted into a pressure vessel which left the compression cylinder open. It was then possible to mount various compression spaces allowing a variety of compression configurations to be investigated.

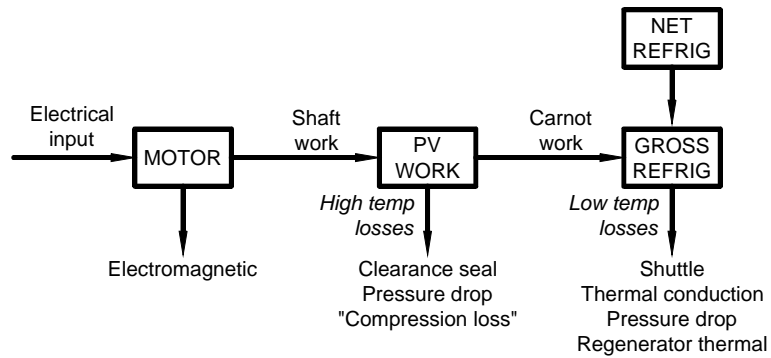


Figure 1. A simplified schematic of the losses in a Stirling cycle cryocooler.

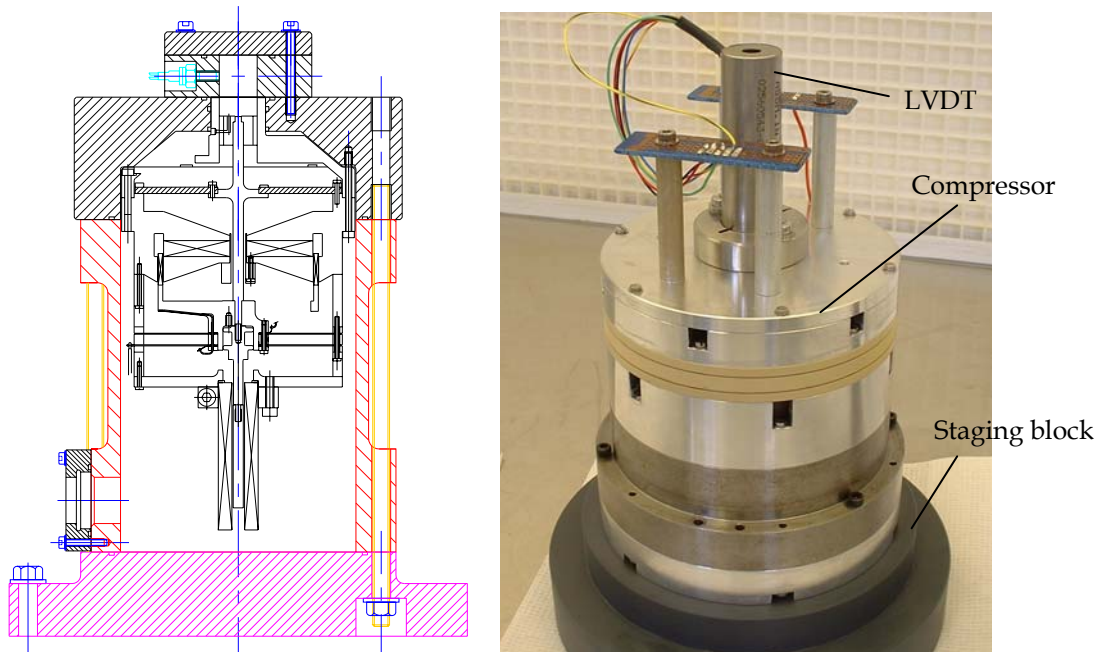


Figure 2. Linear compressor. Left: section view. Right: awaiting assembly onto the mounting plate.

### 3. Instrumentation

In previous measurements of the “compression loss” three main loss mechanisms were not fully characterized: it is assumed that these account for the missing power.

- Heat transfer losses – assumed to be the largest component as this would have the correct dependency on frequency, pressure swing, and swept volume.
- Motor losses (non  $i^2R$ ) – usually assumed small but difficult to measure.
- Windage – usually assumed small and/or equivalent to running in air at atmospheric pressure.

All three of these losses would have to be accounted for in the experimental compressor to achieve a sufficiently good energy balance, even though heat transfer losses were likely to be the largest component. However, measurement of all of these losses is difficult because:

- Heat transfer losses require extremely accurate measurements of the PV-loop in the compressor. This is complicated by the comparatively poor phase performance of conventional LVDT equipment.

- The motor losses can only be independently measured in vacuum. Excessive coil heating limits the maximum current which can be used, making the losses very small. It is then difficult to achieve sufficient accuracy.
- Windage measurements require elimination of compression, usually requiring a rebuild.

It was therefore considered that a major part of this project would consist of developing the ability to accurately make these measurements in a compressor. This required careful sensor calibration, initial characterization, and data processing development before any measurements of heat transfer losses could be attempted.

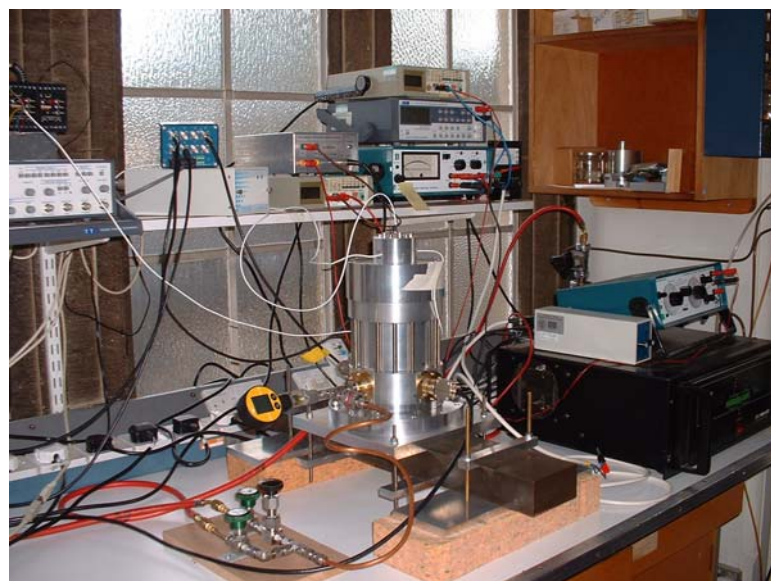


Figure 3. Top: the compressor (note the three pressure transducer cables at the top and the 'top-hat' compression space). Bottom: the test set-up (see layout schematic in figure 9).

### 3.1. Pressure sensors

Measurement of the compression space pressure is crucial for calculating the PV work and it was therefore imperative to identify a pressure sensor with sufficient stability and accuracy. We had initially intended to use a Druck PDCR200 device but a previous study [5] indicated that this might have some problems related to temperature compensation. We therefore selected the Endevco 8510B sensor as being suitable due to its intrinsic temperature compensation, although some issues were raised about its robustness. It was decided to investigate both types of sensor to check which was best for the current study. Three sensors were therefore initially installed in the compression space of the first test configuration: an Endevco 8510B, a Druck PDCR200, and a Druck PDCR200 with a thermal baffle consisting of 7 stainless-steel 150-mesh screens (since the Endevco had a baffle and the Druck did not). The signal processing electronics consisted of a Fylde FE-366-TA bridge amplifier.

The sensors were calibrated using a linear fit as shown in figure 4. During initial operation the output of all three sensors was compared and it became apparent that there was a problem with the frequency domain response of the electronics. It was therefore decided to measure the phase and gain characteristics of the electronics by applying an AC voltage to the amplifier inputs. It quickly became clear that the response was not adequate, with the first pole of the output filter occurring at around 400 Hz rather than 10 kHz as expected. This was traced to the electronics having been incorrectly supplied. After consulting the manufacturer, a replacement component allowed the filter pole to be moved to 10 kHz. After this modification the phase and gain response were measured again, as shown in figure 5, and appeared to be more than satisfactory. By comparing the sensor outputs during initial testing it was concluded that there was no intrinsic problem with either Druck sensor, although the Endevco would be favoured due to its better specifications.

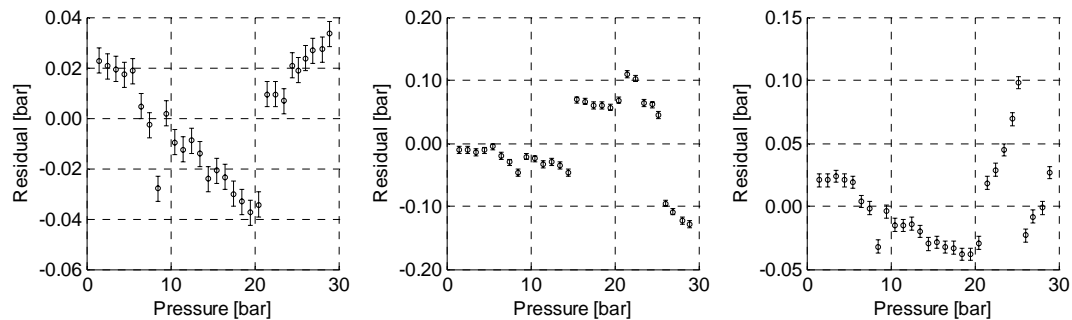


Figure 4. Pressure sensor calibration residuals (linear fit). From left to right: Endevco, Druck-plain, Druck + meshes.

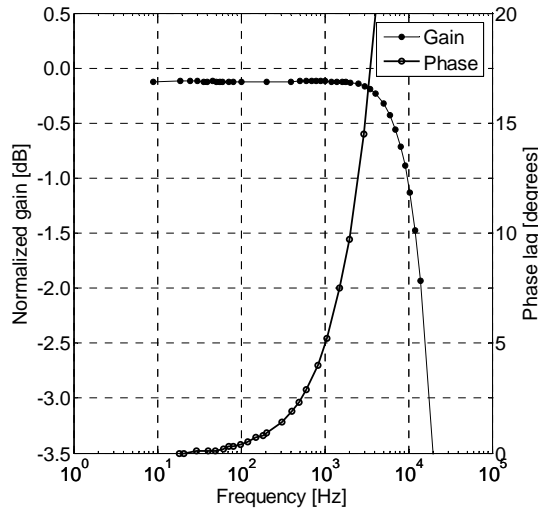


Figure 5. Frequency domain response of the pressure sensor signal conditioning electronics.

### 3.2. Piston position sensor

The piston position sensor was a modified Schaevitz MHR 1000 LVDT controlled by a Schaevitz SMS/GPM-109A signal conditioning module. During previous projects the alignment of the LVDT slug in the LVDT coils was found to be quite difficult and therefore the LVDT slug was modified to be machined at the same time as its supporting structure. This was found to considerably facilitate assembly.

The measurements of the motor position are used to calculate the volume in the compressor and hence the PV loop. It is therefore vitally important that they are accurate in terms of stroke and phase. The stroke calibration was performed against a depth micrometer, the results are shown in figure 6 where a cubic fit has been applied to the data (the cubic terms result from LVDT transformer coupling and not the electronics). The LVDT phase distortion was measured by applying a sine-wave with a DC bias to the inputs (the demodulator essentially rectifies the input according to the modulating signal and therefore purely positive signals pass through unaffected), and results are shown in figure 6 (although see below for more discussion).

### 3.3. Electrical sensors

The current over the coil was measured using a Hall effect sensor unit built for this project. The voltage over the coil was measured using a Fylde 4601A isolating amplifier (in conjunction with a Fylde 261HVA HV attenuator). The phase and gain characteristics were tested by applying a known voltage to a non-inductive resistor in the case of the current sensor, and directly to the sensor in the case of the voltage sensor. The AC responses of the sensors are shown in figure 7, and the calibrations are shown in figure 8.

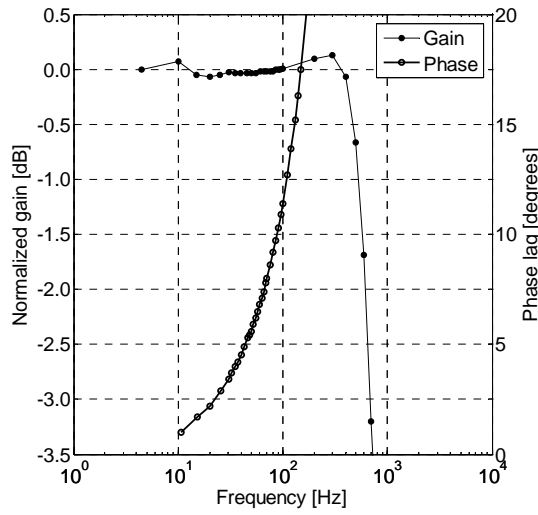
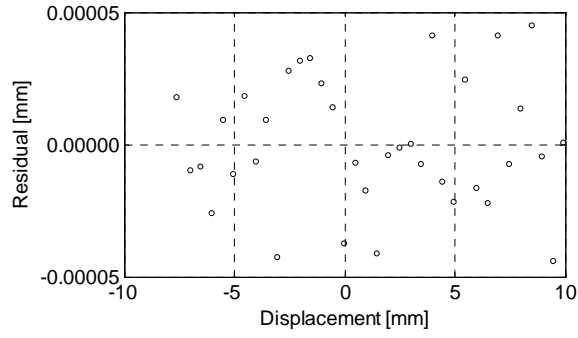


Figure 6. LVDT calibration (cubic fit), and frequency domain response.

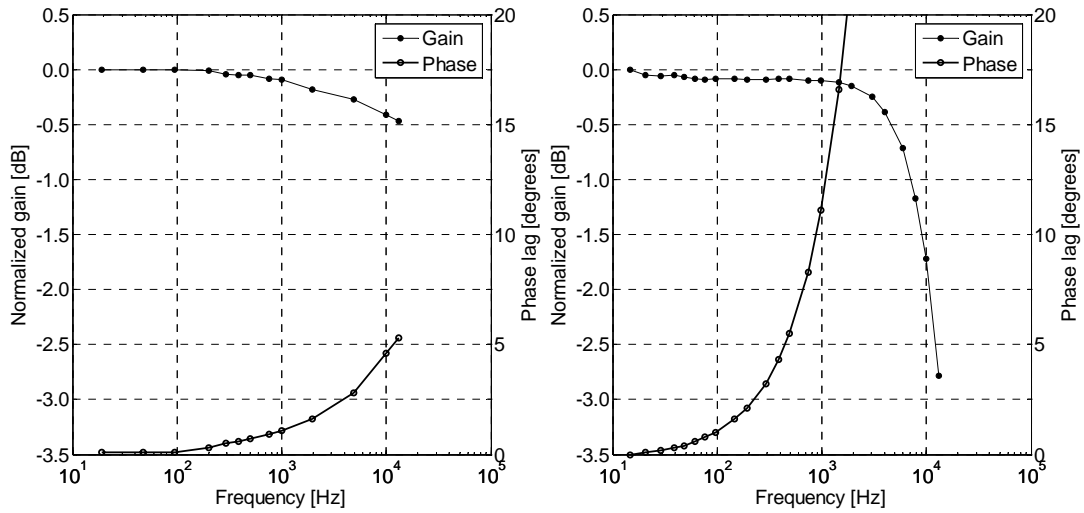


Figure 7. Frequency domain response of the current sensor (left), and the voltage sensor (right).

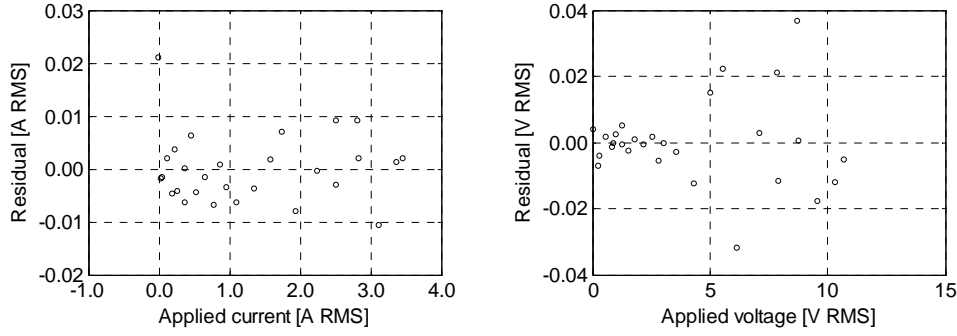


Figure 8. RMS calibration of the of the current sensor (left), and the voltage sensor (right).

### 3.4. Data acquisition and analysis

The data acquisition system was based on an eight channel Fylde Micro-analog 2 USB DAQ. Each channel was sampled in two blocks of four, i.e. channels 1 and 5 were sampled simultaneously, then channels 2 and 6 after 5  $\mu$ s, and so on.

Initial data processing took the form:

1. Remove phase shifts from data caused by the DAQ and the signal processing electronics using the phase responses measured above. This was achieved by shifting each channel by a non-integer number of data points according to the time delay given by the phase shift at the operational frequency. The fractional part of the time shift was calculated by interpolation. This method was chosen because the data were dominated by the fundamental frequency and this method otherwise causes no amplitude or start-up distortion (unlike synthesised 'reverse time' inverse filters).
2. Calculate RMS and DC values (from full cycles).
3. Calculate mean input power ( $\langle vi \rangle$ ), and integrate  $pdV$  by trapezoidal method.
4. Finally, apply calibration factors.

The majority of samples were taken at 25 kHz per channel for 0.2 s.

## 4. Energy balance in the compressor

The electrical power input into the compressor,  $P_{inv}$  is consumed by a number of different loss processes:

- Joule ( $i^2R$ ) losses,  $P_{ir}$  – these are present when the motor is not moving and are characterized by the DC resistance of the coil,  $R_c$ .  $P_{ir}(i_{rms}, i_{dc}, T) = i^2 R_c(T)$ , where  $T$  is the coil temperature.
- AC resistance losses – these are due to several effects including self-inductance of the coil and the frequency dependent skin depth of the coil.  $P_{ac}(f, i_{rms}, T) = i^2 R_{c,ac}(T, f, i_{rms})$ . Where  $f$  is the operational frequency and  $i_{rms}$  is the applied current.
- Eddy current losses – these are primarily due to two effects. The first is the AC current inducing eddy currents in the magnet and supporting structure even when the motor is stationary, these are termed “static motor eddy losses”,  $P_{ms}(T, f, i_{rms})$ . The second loss is due to the motion of the coil passing through a magnetic field inducing eddy currents in the coil holder and support structure. These are termed “moving motor losses”,  $P_{mm}(T, f, i_{rms}, x_{rms}, x_{dc})$ . Where  $x_{rms}$  is the RMS stroke and  $x_{dc}$  is the motor position offset.
- Vibrational losses,  $P_{vib}$  – these are caused by the moving mass of the motor exciting the support structures of the motor and entire compressor. These are likely to be dependent on the stroke and the frequency,  $P_{vib}(f, x_{rms})$ .
- Frictional losses,  $P_{fric}$  – due to sliding friction or stiction between the piston and bore. Likely to be dependent on the stroke and frequency,  $P_{fric}(x_{rms}, f)$

- Hysteresis losses in the springs,  $P_{shys}$  – bending in the springs is unlikely to be truly reversible and consumes power dependent on the frequency and stroke,  $P_{shys}(x_{rms}, f)$ .
- Hysteresis losses in the magnet,  $P_{mhys}$  – due to the reversing current affecting the magnetization of the magnet.
- “Windage”,  $P_w$  – this is caused by fluid shear between the moving components and ambient gas. It is present when there is no compression and should be dependent on piston velocity and filling pressure.
- Piston gas shear force loss – there will be a net shear force between the moving piston and static bore according to the gas viscosity,  $P_{shear}(T, f, x_{rms}, p_{fill})$ . This will be distinct from the shear force imparted by the moving gas which is accounted for in the clearance seal loss.
- Turbulent gas motion,  $P_{turb}$  – as the piston moves through the gas it can shed eddies into the gas off its edges (due to the shear force on the gas being non-continuous at this point). This should be dependent on the gas pressure (via the density), viscosity, and piston velocity,  $P_{turb}(T, f, x_{rms}, p_{fill}, p_{rms})$ .
- Seal loss,  $P_s$  – this is caused by the bulk flow of gas through the clearance seal into the compressor body. Since the pumping of gas causes mass to be lost and gained in the compression space this loss appears as part of the PV work,  $P_s(f, p_{fill}, p_{rms}, T)$ .
- Heat transfer loss in the compression space,  $P_{hx}$  – this is caused by the imperfect transfer of heat between the walls of the compression space and the gas, and is probably dependent on the filling pressure, pressure swing, frequency, temperature, and stroke/piston offset (since this determines the area of cylinder wall with which heat can be transferred),  $P_{hx}(f, T, p_{fill}, p_{rms}, x_{rms}, x_{dc})$ .

The full power balance can therefore be written as:

$$P_{in} = P_{ir}(i_{rms}, i_{dc}, T) + P_{ac}(f, i_{rms}, T) + P_{ms}(T, f, i_{rms}) + P_{mm}(T, f, i_{rms}, x_{rms}, x_{dc}) + P_{vib}(f, x_{rms}) + P_{fric}(x_{rms}, f) + P_{shys}(x_{rms}, f) + P_{mhys} + P_{shear}(T, f, x_{rms}, p_{fill}) + P_w(T, f, x_{rms}, p_{fill}, p_{rms}) + P_{turb}(T, f, x_{rms}, p_{fill}, p_{rms}) + P_s(f, p_{fill}, p_{rms}, T) + P_{hx}(f, T, p_{fill}, p_{rms}, x_{rms}, x_{dc}) + P_{load} \quad (1)$$

Where the power actually delivered to any load has been written as  $P_{load}$  (zero in the current application).

Clearly the power balance is actually very complicated and from an experimental point of view it is useful to break the power into three components: the Joule loss, the “motor loss”, and the “PV work”, i.e. the work done by the gas in the compression space.

$$P_{in} = P_{ir}(i_{rms}, i_{dc}, T) + P_{motor} + P_{gas} \quad (2)$$

Where:

$$P_{motor} = P_{ac}(f, i_{rms}, T) + P_{ms}(T, f, i_{rms}) + P_{mm}(T, f, i_{rms}, x_{rms}, x_{dc}) + P_{vib}(f, x_{rms}) + P_{fric}(x_{rms}, f) + P_{shys}(x_{rms}, f) + P_{mhys} + P_w(T, f, x_{rms}, p_{fill}, p_{rms}) + P_{turb}(T, f, x_{rms}, p_{fill}, p_{rms}) + P_{shear}(T, f, x_{rms}, p_{fill}) \quad (3)$$

$$P_{gas} = P_s(f, p_{fill}, p_{rms}, T) + P_{hx}(f, T, p_{fill}, p_{rms}, x_{rms}, x_{dc}) + P_{load} \quad (4)$$

It is conventionally assumed that  $P_{motor}$  is small in typical Stirling cycle type machines but since  $P_{gas}$  is also likely to be quite small in the present application (with no ‘load’), it is significant. For the present it will be assumed that the following losses are negligible or represented in the other losses:  $P_{ac}$  (at low frequencies, see appendix A),  $P_{vib}$ ,  $P_{fric}$  (needs to be confirmed by a bounce test),  $P_{shys}$ ,  $P_{mhys}$  (because the permanent magnetic field is much greater than the coil’s field),  $P_{turb}$  (since the piston speeds are comparatively low), and  $P_{shear}$  (piston diameter is small, see appendix A).

## 5. Preliminary tests

### 5.1. Initial check-out

After assembly and removal from the clean room the compressor was attached to the testing facility shown in figure 3. To confirm that no damage had been done to the alignment a ‘bounce test’ was performed in vacuum, at least 35 bounces were observed, and it was therefore concluded that the piston was sufficiently free and that the sliding friction losses between the piston and cylinder,  $P_{\text{fric}}$ , were negligible.

### 5.2. Testing in vacuum

From the above power balance the “motor losses” can be further broken down into those which occur with gas present and those which occur in vacuum.

$$P_{\text{motor}} = P_{\text{motor,gas}} + P_{\text{motor,vac}} \quad (5)$$

$$P_{\text{motor,gas}} = P_{\text{w}}(T, f, x_{\text{rms}}, p_{\text{fill}}, p_{\text{rms}}) + P_{\text{turb}}(T, f, x_{\text{rms}}, p_{\text{fill}}, p_{\text{rms}}) \quad (6)$$

$$P_{\text{motor,vac}} = P_{\text{ms}}(T, f, i_{\text{rms}}) + P_{\text{mm}}(T, f, i_{\text{rms}}, x_{\text{rms}}, x_{\text{dc}}) \quad (7)$$

Static motor losses were determined when the compressor was manufactured and it was assumed that these had not changed. These measurements were found to fit the equation:

$$P_{\text{ms}} = a f^{3/2} i_{\text{rms}}^2 \quad (8)$$

where  $a = 3.50\text{E-}04 \pm 5.20\text{E-}06 \text{ WHz}^{-3/2}\text{A}^{-2}$ . The form of this relationship is to be expected if the motor is treated as two circuits, comprising the motor coil and the pole-pieces, linked by a mutual inductance (see appendix A). It should be noted that the error on the above fit was quite large because the original data was taken at low currents to avoid damaging the coil and the error bars were significant.

The first experimental tests were performed by running the motor in vacuum with the goal of measuring the remaining components of the motor loss. The motor was operated whilst measuring the input voltage, current, power, and stroke as shown in figure 9. The coil resistance was then determined by passing the equivalent DC current through the motor when stationary. The  $i^2R$  loss and the stationary eddy current loss were calculated and the remainder of the input power was attributed to the moving motor loss, i.e.

$$P_{\text{mm}} = P_{\text{vi}} - i^2R - P_{\text{ms}} \quad (9)$$

This appeared to correlate reasonably well with the RMS motor velocity, as shown in figure 10, and this is to be expected from the mechanism of eddy current generation. The data appeared to be reasonably well fitted by:

$$P_{\text{mm}} = c_1 u_{\text{rms}} + c_3 u_{\text{rms}}^3 \quad (10)$$

where  $u_{\text{rms}} = 2\pi f x_{\text{rms}}$  (see below for the fitted values).

The biggest problem with these measurements is via  $P_{\text{ms}}$  and the limited current range used (and hence stroke and frequency). This is because in vacuum the heat is not readily removed from the coil, unlike during operation with gas, where the gas provides excellent cooling to the moving coil. This therefore leads to the “in-vacuo” data being over a smaller range of operating parameters than are actually used in an operational machine and it is therefore necessary to extrapolate this data somewhat (e.g. the maximum current used in vacuum was 1 A whereas, to date, up to 2 A has been used when filled with gas).

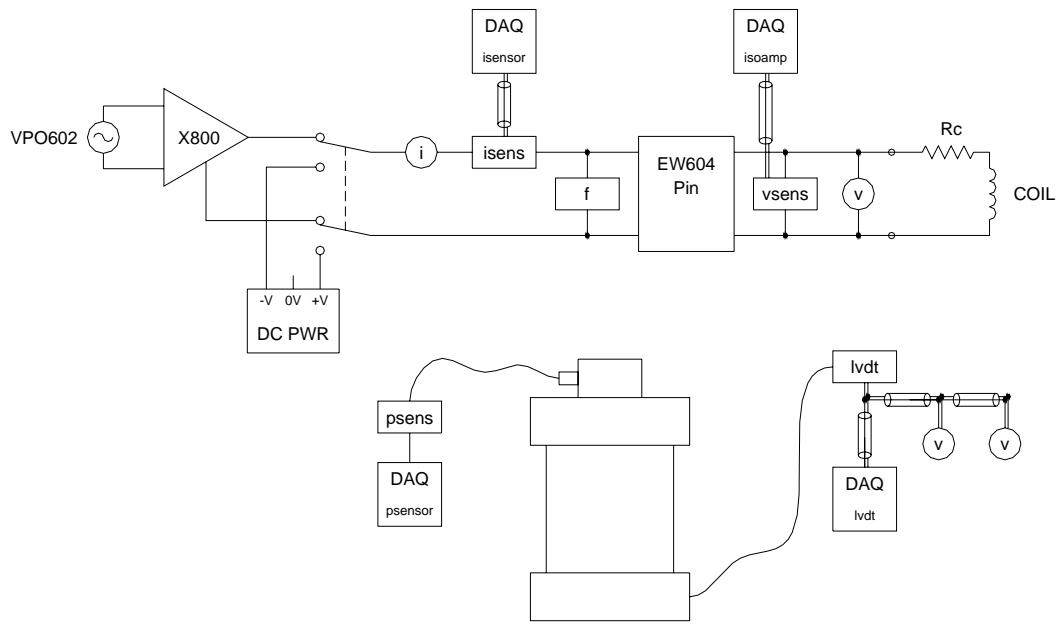


Figure 9. Testing set-up electrical schematic. The input signal is generated by a frequency generator (Feedback VPO602), which controls an AC amplifier (HH X800). This is then connected to the system by a DPDT switch which allows a DC power supply to be connected when required. Two Fluke 8010A DMMs are used for current and voltage sensing, whereas a TTI 1705 DMM is used for frequency measurement. The Feedback EW604 power meter is used to give an immediate measurement of input power. All sensors are connected to the Fylde DAQ system.

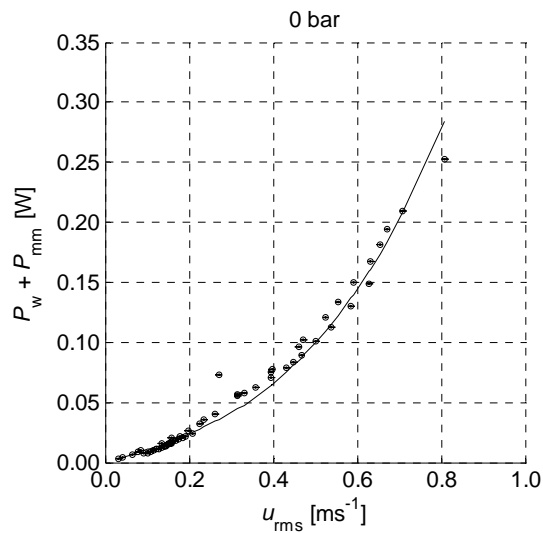


Figure 10. Moving motor loss with piston RMS velocity (as measured in vacuum).

### 5.3. "Windage" measurements

The final power loss which does not occur as part of the PV-loop is 'windage'. This is usually assumed to be small or is measured by running the motor in air, but it is non-trivial to derive analytically since any flow is limited to the boundary layer and is unsteady. To investigate this loss the compression chamber was removed and replaced with a 0.5" diameter copper pipe connected to the space behind the piston, as shown in figure 11. This prevented compression from occurring but allowed the compressor to be filled with gas to working pressure (thus allowing a much more accurate analysis than most previous studies).



Figure 11. Windage measurement configuration.

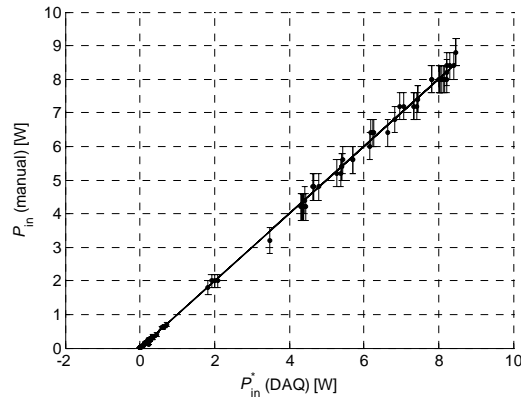


Figure 12. Manually and DAQ measured input power.

Measurements of the sum of the moving motor loss and windage loss were made at various strokes and frequencies using helium and nitrogen up to 25 bar filling pressure, calculated using:

$$P_w + P_{mm} = P_{vi} - i^2R - P_{ms} - P_{gas} \quad (11)$$

where the coil resistance was measured for each operating point by quickly reducing the motor drive current to zero and switching to a DC power supply to provide a “4-wire” resistance measurement. The gas power was also included in the calculation since for highest frequency tests with nitrogen a small PV-loop was observed; although the area was smaller than the errors in all cases.

Figure 12 shows a comparison between the electrical input power calculated from the DAQ measurements and that measured using the (rather low resolution), power meter (to a higher power level than was possible in vacuum). A good correlation was observed, within the error bars, indicating that the DAQ measurements were reliable.

Figure 13 shows some of the windage loss measurements in helium and nitrogen plotted versus RMS piston velocity. It can be seen that, as expected, the windage losses are much larger for nitrogen due to its greater density. It can also be seen that the errors are quite large at high velocities. This is because of the errors on the static motor loss. During these tests the motor resonance was observed at 25 Hz, the value also observed in vacuum. This meant that to obtain high strokes at high frequencies, i.e. high velocities, a large current had to be supplied to the coil. Since the static motor loss is proportional to the square of current this gave rise to the large errors. It was found that all of these measurements fitted reasonably well to:

$$P_w + P_{mm} = c_1 u_{rms} + c_3 u_{rms}^3 \quad (12)$$

where  $c_3$  was no longer constant, as in the vacuum case. By plotting the fit coefficients, including those from the in vacuo measurements it was found that  $c_3$  depended on the inverse kinematic viscosity in an approximately linear manner, as shown in figure 14:

$$\begin{aligned} c_3 &= c_{30} + c_{31} \rho / \mu \\ &= c_{30} + c_{31} / \nu \end{aligned} \quad (13)$$

The final term is what might be expected from a pressure drop type of windage (a pressure difference proportional to  $u^2$ , giving a power dissipated proportional to  $u^3$ ). Therefore it was concluded that the moving motor and windage losses were given by:

$$P_{mm} = c_1 u_{rms} + c_{30} u_{rms}^3 \quad (14)$$

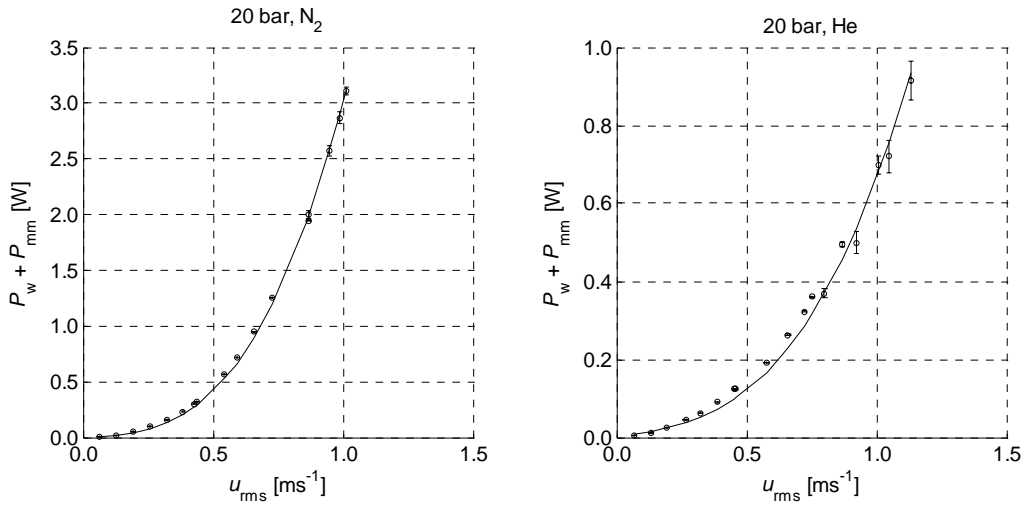


Figure 13. Fits for  $P_w + P_{mm}$  with nitrogen (left), and helium (right) at 20 bar filling pressure.

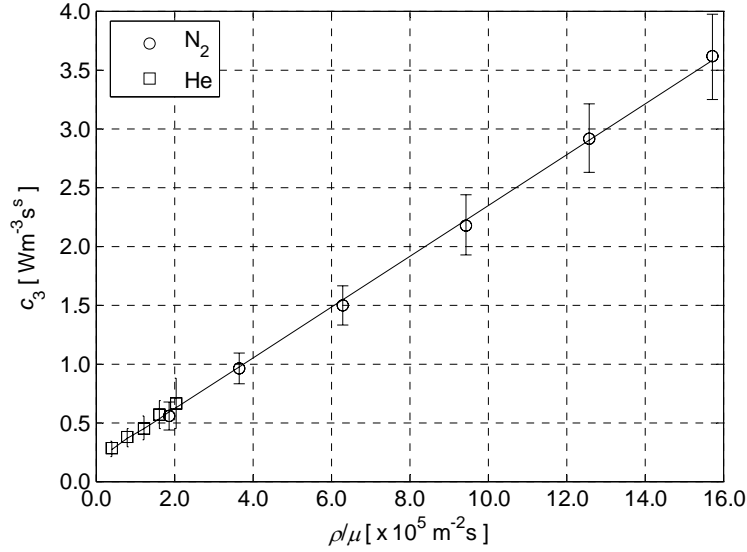


Figure 14. Linear fit to the  $c_3$  coefficient versus reciprocal kinematic viscosity (note that error bars are probably overestimated).

$$P_w = c_{31} u_{\text{rms}}^3 / \nu \quad (15)$$

Where  $c_1 = 0.1031 \text{ Wm}^{-1}\text{s}$ ,  $c_{30} = 0.1882 \text{ Wm}^{-3}\text{s}^3$ , and  $c_{31} = 0.2135 \times 10^{-5} \text{ Wm}^{-1}\text{s}^2$ .

#### 5.4. Verification of the PV loop measurements

With the motor losses characterized the PV-loop related losses could be investigated. These could be calculated using two methods: via the losses subtracted from the total input power, or via the PV-loop area. To obtain a good energy balance, and to characterize any additional losses, however, both were used and this required verification of the method of calculating the PV-loop (including phase correction and integration).

##### 5.4.1 In-software tests

The first testing method was to numerically simulate a continuous PV loop, simulate digitization and phase shifting, and then run through the integration system. The outputs were then compared to the inputs. Good agreement was found, indicating that, at least at the software level, the data processing was accurate.

##### 5.4.2 Signal processing electronics: loop-tests

The second testing method was to electrically simulate a PV-loop using phase shifted sinusoidal voltages applied to the signal processing electronics using the arrangement shown in figure 15. The measured outputs were then compared to the input voltages and phase shifts to determine the accuracy. A frequency generator was used to create two sine-waves with variable phase shift and amplitude. The first of these signals was passed into the pressure sensor signal processor (which essentially was an instrument amplifier followed by a filter), both input and output were recorded using the DAQ as PIN and POUT. The LVDT signal was DC shifted as above and the input/output signals were recorded as LVDTIN and LVDTOUT. Using this arrangement it was therefore possible to simulate a PV-loop and measure the integrated area before and after the signal conditioning electronics. The following results could be derived from this data:

- By adapting the data analysis system to alter the phase correction of the LVDT signal until the integration of the output signals agreed with the expected (analytic), integral value, the LVDT phase shift could be measured, as shown in figure 16. It was found that a slightly lower value of the LVDT phase shift than had previously been measured above

was required to obtain good correlation, corresponding to a constant time delay of approximately 20  $\mu$ s. To test that this was not caused by any delay between channel samples an identical signal was applied to all channels and the time difference between samples measured on the computer, the results were found to agree with the time delays stated by the DAC manufacturer.

- The input signals (PIN and LVDTIN), were also integrated and compared to the analytic values to check the integration algorithm, good agreement was always found and it was therefore considered to be robust and accurate.
- Finally, the phase shifts between input and output signals could be calculated and compared to those measured from the integration method above. Excellent agreement was found indicating that the calculated values were correct.

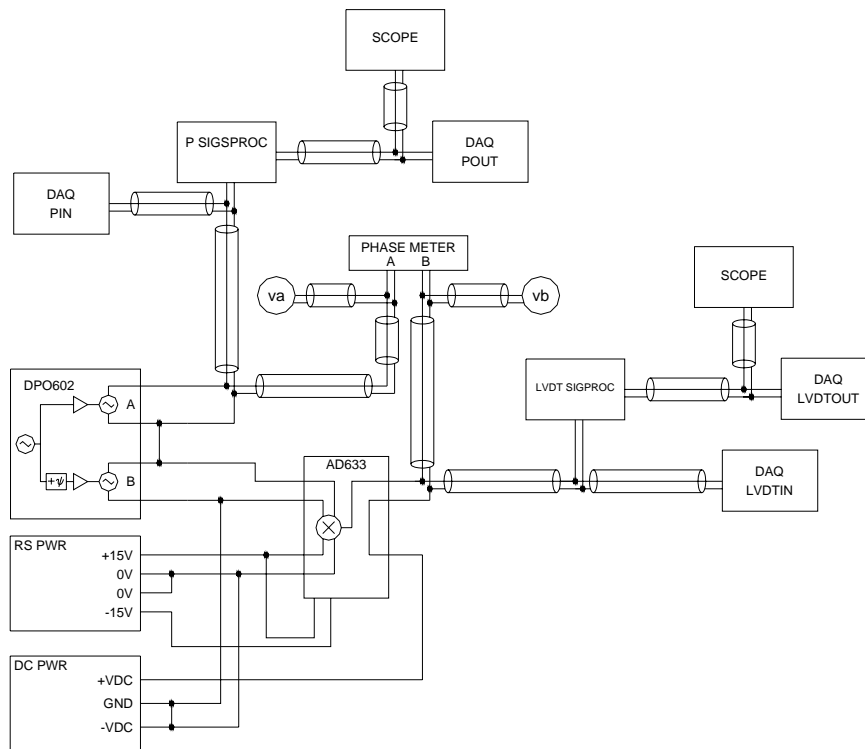


Figure 15. "Loop test" arrangement. Note that the AD633 multiplier is used to produce a bias, rather than as a discrete gain stage.

#### 5.4.3 Signal processing electronics: patch-tests

The final method of measuring the LVDT phase shift was to patch into the LVDT cable and directly sample the input of the LVDT signal processing electronics (i.e. an AM signal), whilst the compressor was running. A MatLab program was written to demodulate the signal without any phase distortion (this is possible using filtering in the frequency domain by applying the filter both forwards and backwards in time to prevent phase distortion). The demodulated signal could then be compared to the output from the signal processing electronics. The compressor was run between 14.5 Hz and 60 Hz in-vacuo and the results are shown in figure 16. It can be seen that there is some increased scatter at high frequencies and this is likely to be due to the requirement of keeping the current low in vacuo leading to small strokes/signals at high frequencies, far away from resonance.

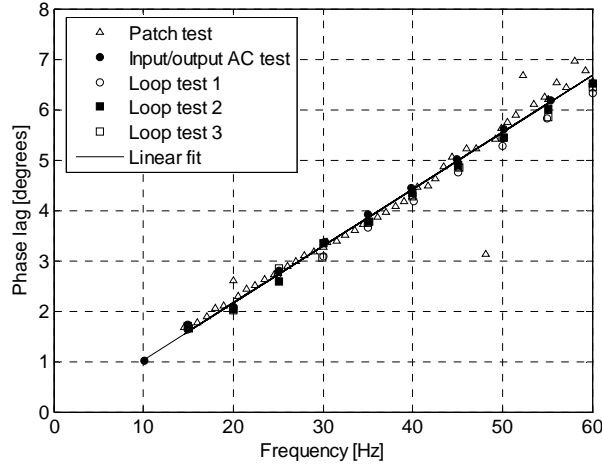


Figure 16. LVDT phase shift results (linear fit applied to all data).

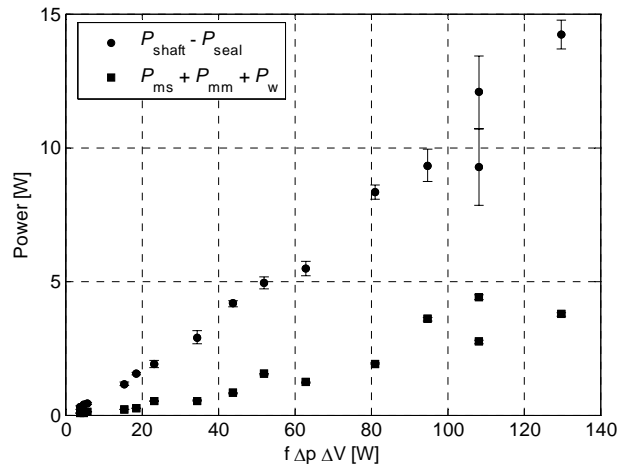


Figure 17. Comparison of the 'compression loss' in the original compressor cryocooler configuration (seal losses have been estimated from current seal gap measurement), and motor/windage losses as currently measured.

#### 5.4.4 Conclusions

It was concluded that the integration and phase correction processes were accurate and robust. It did appear, however, that the LVDT phase did not quite agree with the previously measured values, this was attributed to some small error in the digital phase meter which was previously used.

### 6. Comparison of windage/motor losses to compression loss measurements in original cooler configuration

At this stage it was felt that the motor, windage, and PV-loop measurement system had all been sufficiently well characterized to enable accurate PV-loop measurements to be made. However, it was first interesting to compare the size of these losses to measurements made of the 'compression loss' in the compressor's original configuration as part of a cryocooler (which did not include a compression space pressure sensor). As shown in figure 17, it was found that between 16 and 30% of the 'compression loss' could be accounted for by the fitted forms of  $P_{mm} + P_{ms} + P_w$  and it therefore appears that these losses are more significant than had previously been thought (since these losses had not been included in the original cooler analysis). An important question is therefore, why have these losses not been observed before? It is suspected that there are three reasons for this:

- The extra motor losses, not previously characterized, are proportional to the total work done by the gas, i.e. they are proportional to  $f\Delta P\Delta V$ . It is therefore easy to see how, without direct PV-loop measurements, they might be assumed to be part of the PV-loop.
- The phase characterization of the pressure sensor and LVDT must be done extremely carefully and even small errors could lead to apparent systematic increases or decreases in the observed PV-work. Therefore even if pressure sensors had been installed it would be easy to ignore these losses as a distinct source of power consumption.
- The motor loss increases rapidly with speed and current. Since previous motor loss measurements have typically been performed in air at 1 bar or in vacuum, however, low currents and speeds have been used due to concerns over coil heating. These losses would therefore have appeared to be much smaller in previous studies.

## 7. Compression measurements

The next step was to measure the power balance in the compressor with a dead volume attached. A plain 'top hat' cylinder head was therefore attached giving a total mid-piston volume of 7.4 cc. The compressor was operated as previously: stroke and frequency were set and the compressor was allowed to come into equilibrium (i.e. piston offset pumping), data was then acquired, the drive supply was then quickly disconnected, a DC current applied (100 mA), and a longer (10s at 1kHz), data file was acquired to measure the coil resistance.

At the time of writing the following measurements with helium have been completed:

- Frequency swept from 20-60 Hz, stroke constant: 33% and 50% stroke at 5 bar and 10 bar.
- Frequency constant, stroke swept: 25, 40, 55 Hz at 5 bar and 10 bar.

Figure 18 shows the measurements with the stroke held constant. It was expected that two processes would account for the PV-loop power: the seal loss and a heat transfer loss. The seal loss has been calculated based upon the assumption of a constant seal gap and ignoring piston velocity. The heat transfer loss has been estimated from the formula of Cooke-Yarborough and Ryden (CYR) [7]. Both of these losses are described in appendix A. We note the following about these results:

- At lower stroke the power delivered and the PV-loop power agree well at 5 bar but this does not appear to be the case at higher stroke or pressure, where the difference appears to be roughly independent of frequency.
- The estimated components of the PV-loop power do not agree with the PV-loop power, however, the magnitude of disagreement is not great. It should be noted that the only available experimental comparison of the CYR formula was performed by Kornhauser and Smith [4], and they found that the CYR formula (which was considered to agree best with their measurements), disagreed by as much as 30% with their data. It should also be noted that the CYR formula does not account for the exchange of gas with the seal or any heat transfer associated with it.

To further investigate why the PV-loop power and the delivered power did not agree at the higher stroke, the frequency was held constant and the stroke increased. The maximum stroke was restricted in all tests by the clearance available at top dead centre (TDC), as the compressor was driven by a purely AC amplifier. At higher strokes the pressure swing was larger in the compression space and the 'DC pumping effect' on the piston (see appendix A), was increased pushing the piston towards TDC. This problem is exacerbated at higher frequencies as the compression process becomes more adiabatic and the pressure swing to stroke ratio increases. The results from these tests are shown in figure 19. It can be seen that  $P_{del}$  and  $P_{gas}$  tend to diverge at higher strokes. This would indicate an additional loss mechanism drawing power from the motor before it reaches the compression gas, possibilities include:

- Compression in the space behind the piston. There is a pressure sensor in the pressure vessel but it is not currently close enough to measure this accurately. Given the likely pressure swing, however, it is unlikely that this could account for the magnitude of the loss.
- Additional windage losses. This could be due to some form of windage associated with the piston, since the additional loss occurs during compression, although it should have been taken into account in the seal loss (and the shear force is negligible).
- Existing motor losses varying with the piston offset position (which, as discussed above, was not constant). This could be investigated by using a DC amplifier to run the motor at different offset positions, or at least keep it central.

Finally it should again be noted that the magnitude of disagreement between  $P_{del}$  and  $P_{gas}$  is not great (up to 20%).

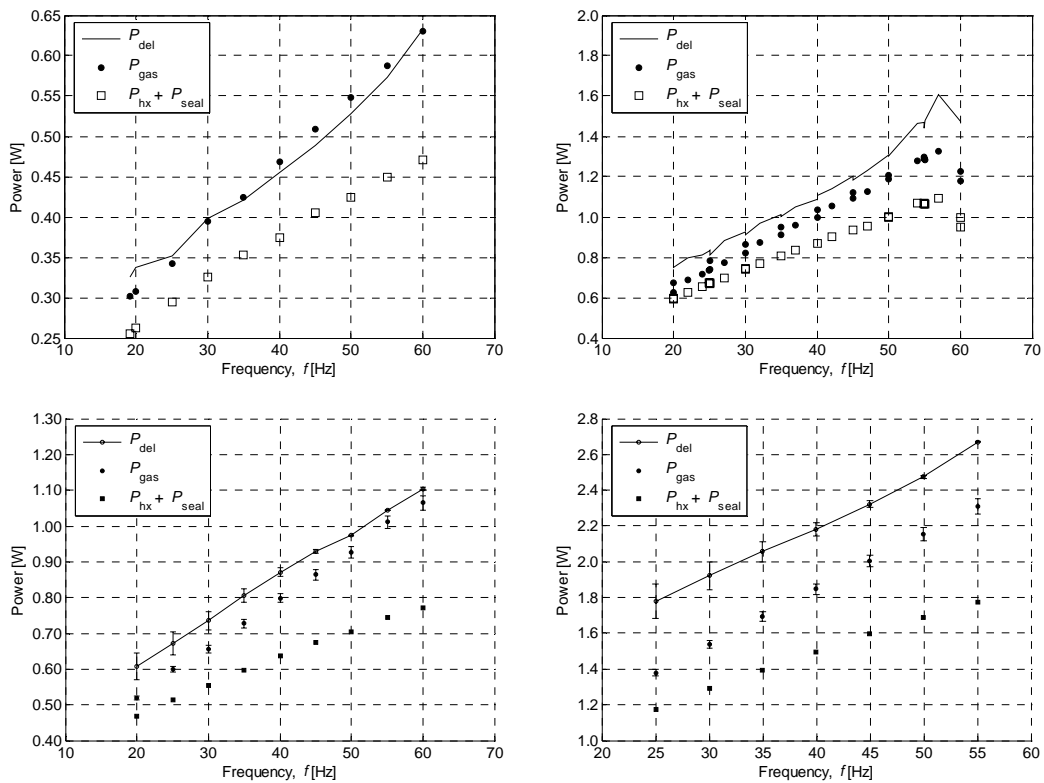


Figure 18. Power with varying frequency measured at 5 bar (top) and 10 bar (bottom), with stroke held constant at 33% (left) and 50% (right). Note that the dip in power at 60 Hz at 50% stroke is because the stroke was reduced to avoid striking the end stops. For the data-set at 10 bar errors have been estimated for  $P_{gas}$  by assuming an error on the phase correction of  $\pm 0.05^\circ$ , and a constant current supply was used for the resistance measurements to improve accuracy.

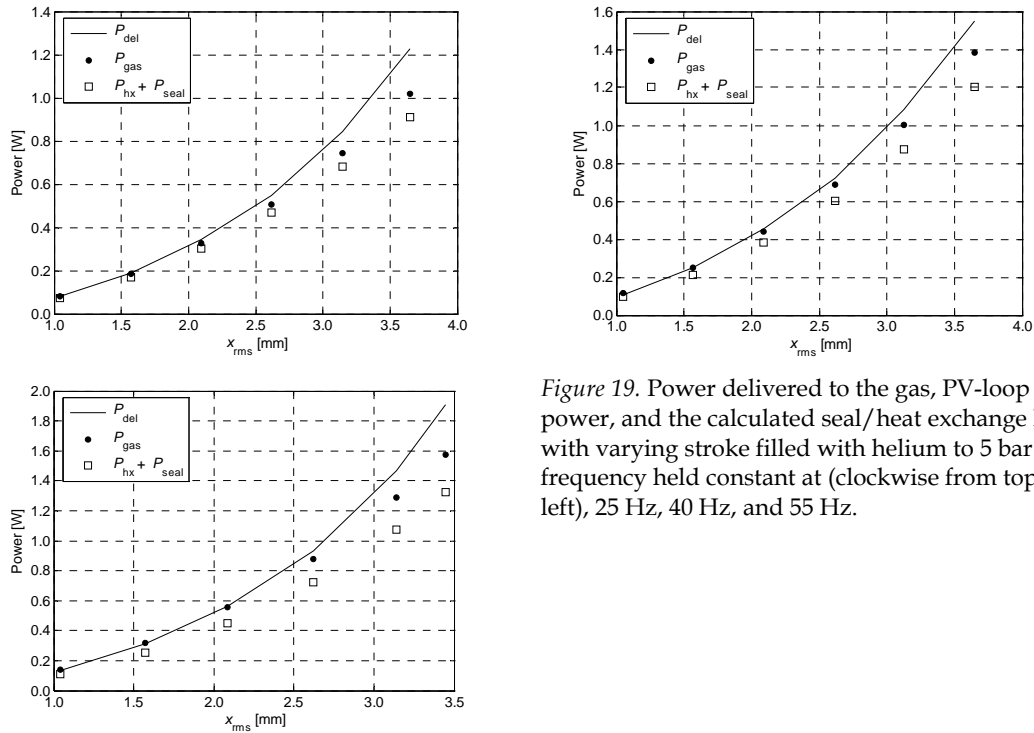


Figure 19. Power delivered to the gas, PV-loop power, and the calculated seal/heat exchange loss with varying stroke filled with helium to 5 bar and frequency held constant at (clockwise from top left), 25 Hz, 40 Hz, and 55 Hz.

## 8. Conclusions

The aim of this work was to investigate unexplained losses in cryocoolers which were assumed to be thermodynamic in nature. Initially this required development of an extremely well calibrated measurement system and commissioning of a linear compressor. To enable a sufficiently good energy balance to be produced electromagnetic motor losses and windage were measured and it immediately became clear that these were more significant than had previously been assumed. In previous studies measurements made in vacuum at low currents and speeds, as well as measurements in air at 1 bar, had indicated that the losses were negligible but this did not take into account the strong dependence on current, frequency, and motor speed. With these new measurements it is clear that at least part of the “compression loss” is not thermodynamic in nature. Although we have not yet developed an analytic theory of these losses it is hoped that further work, possibly involving FEA based electromagnetic simulations may allow a changes to be made to the design of the motor to reduce the losses. It would also be extremely interesting to perform CFD work to investigate the windage loss and possibly reduce it. It would also be very interesting to make measurements on a machine of more recent motor design. Although these are more efficient there is no indication that there should be any fundamental differences and, in fact, the loss might be greater because the motor in the current machine has a plastic coil holder.

One fundamental problem with previous studies was that neither clearance seal losses or the heat transfer losses predicted by the CYR formula could explain the size of the loss as measured (usually) electrically. With the addition of the increased motor losses the agreement was much better and the difference with the measured data was actually rather good (or as good as the previous experimental study of Kornhauser). It is clear that the CYR approach is also not quite correct for clearance seal based cryocoolers due to the flow of gas through the clearance seal which probably causes additional heat transfer losses. A more comprehensive theory might therefore be expected to improve the agreement with the measured data. Alternatively CFD work might be used if an analytic theory cannot be produced. Measurements of the power delivered to the gas and measured from the PV-loop indicated that high strokes there was still a small discrepancy and there are several possible reasons for this which require further investigation.

This work has solved part of the “compression loss” problem but there are still many possibilities for future work:

- Further loss tests to obtain data over a wider variety of operating conditions and cylinder volumes. Also using a DC amplifier to control the piston offset position and investigate higher strokes.
- A thorough error analysis to improve confidence in the existing work.
- New theories to be developed to explain the form of the losses.
- Attempting to quantify the additional “motor losses” which occur during compression.
- Improvements to hardware to reduce possible sources of error (e.g. better LVDT conditioning electronics).
- CFD work to investigate both the heat transfer losses and the windage losses. We are currently developing such a model using Fluent.
- Electromagnetic FEA analysis of the motor to investigate the eddy losses and hopefully reduce them in future designs.
- Investigation of how these losses scale to a geometry closer to that in a full Stirling or pulse tube cooler. This will involve the addition of a discrete load such as a regenerator.

## References

- [1] Orłowska, AH and Davey, G. "Measurement of losses in a Stirling cycle cooler". *Cryogenics*. 27. 645–651. 1987.
- [2] Green, RH, Bailey, PB, Roberts, L, Davey, G. "The design and testing of a Stirling cycle domestic freezer", *Applications for Natural Refrigerants*, International Institute of Refrigeration, Aarhus, Denmark (1996), pp. 2.11–2.15.
- [3] Reed J, Davey G, Dadd, M and Bailey, P. "Compression Losses In Cryocoolers". 13th International Cryocooler Conference. 2004
- [4] Kornhauser, AA and Smith Jr., JL. "A comparison of cylinder heat transfer expressions based on prediction of gas spring hysteresis loss". *Fluid flow and heat transfer in reciprocating machinery*. ASME. 1987.
- [5] Reed J, Dadd M, Bailey P, Petach M, Raab J. "Development of a valved linear compressor for a satellite borne J-T cryocooler". Submitted to *Cryogenics*.
- [6] Stoll, R. "The analysis of eddy currents". Clarendon Press. 1974.
- [7] Cooke-Yarborough, EH and Ryden, DJ. "Mechanical power losses caused by imperfect heat transfer in a nearly-isothermal Stirling engine". *Proceedings of the 20<sup>th</sup> Intersociety Energy Conversion Engineering Conference*. 1985.

## Table of notation

### *Roman alphabet*

$a$	Loss coefficient in $P_{ms}$
$c_1, c_2$	Loss coefficients in $P_{mm}$
$f$	Frequency
$i$	Current
$p$	Pressure
$P$	Power
$R$	Resistance
$T$	Temperature
$u$	Velocity
$v$	Voltage
$V$	Volume
$x$	Position of motor/piston

### *Greek alphabet*

$\phi$	Crank angle
$\mu$	Viscosity
$\nu$	Kinematic viscosity, $\mu/\rho$
$\rho$	Density
$\psi$	Phase angle

### *Subscripts*

ac	AC loss
c	Coil
dc	DC component of the value
del	Power delivered by motor to the gas, measured electrically and from losses.
ed	Eddy current losses
fill	Filling value
fric	Frictional losses
gas	Power delivered by motor to the gas, measured from the PV loop.
hx	Heat transfer value
in	Total input power
ir	$i^2R$ loss
load	Power delivered to any defined load
mhys	Hysteresis in the motor
mm	Losses when motor is moving
motor	Power consumed by motor losses
ms	Losses when motor is stationary
rms	RMS AC value
s	Seal loss
shys	Hysteresis in the springs
turb	Turbulent
vi	Electrical power delivered to the motor
vib	Vibration
w	Windage

## Appendix A. Expressions used to calculate the losses

### A.1. Derivation of the form of the static motor losses

To obtain an estimate of the form of the static motor loss we treat the problem as comprising two circuits: one consisting of the coil, with a nominal DC resistance  $R_1$ , and the other consisting of some resistance,  $R_2$ , representing the impedance of the metal-work to the eddy currents induced. These circuits are linked by a mutual inductance  $M$ , any self-inductance will be ignored, as shown in figure A1. Note circuit 2 will also be assumed to have an insignificant effect on circuit 1. If there is no relative motion then the emf induced in circuit 2 is:

$$\varepsilon_2 = -M \frac{dI_1}{dt} \quad (\text{A1})$$

If the voltage in circuit 1 is sinusoidal and given by  $v_1 \cos(\omega t)$  then the instantaneous current in circuit 2 is:

$$i_2 = \frac{M\omega}{R_1 R_2} v_1 \sin(\omega t) \quad (\text{A2})$$

The  $i^2 R$  loss in circuit 2,  $P_2$ , is then:

$$P_2 = \frac{M^2 \omega^2}{R_2} i_{1,\text{rms}}^2 \quad (\text{A3})$$

Where  $i_{1,\text{rms}}$  is the RMS current in circuit 1. Now we must consider what  $R_2$  represents: it is given by the resistance of the part of the magnetic circuit through which the eddy current flows. Although it is difficult to identify the physical location of the currents they will be affected by the skin depth of the AC eddy currents. Since  $R = \rho_\Omega l / A$ , where  $\rho_\Omega$  is the resistivity,  $l$  is the length of the current carrying element, and  $A$  is its area:

$$R \propto \frac{1}{\delta} \quad (\text{A4})$$

Where  $\delta$  is the skin depth, which is proportional to  $\delta^{1/2}$ . Hence the eddy current loss power would be expected to be of the form:

$$P_2 \propto f^{3/2} i_{1,\text{rms}}^2 \quad (\text{A5})$$

where  $f$  is the frequency of excitation.

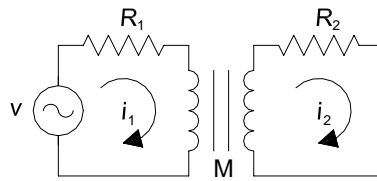


Figure A1. Circuit used to derive the form of the static motor losses.

## A.2. Clearance seal loss

First a simple analysis will be derived for the case of a concentric piston and cylinder. The flow through the seal will be assumed laminar and steady (even though it is in fact sinusoidal). This is justified by the low gas velocities (typically below 10 m/s), compared to the speed of sound in the working fluid (usually helium where  $c = 1010$  m/s). In this case the flow equation is given by:

$$\nabla p = \mu \nabla^2 u \quad (\text{A6})$$

Where  $p$  is the gas pressure,  $\mu$  is the gas viscosity, and  $u$  is the gas velocity. Consider an element of the gap as shown in figure A2. Since the gap dimension,  $\tau$ , is much smaller than the piston diameter,  $D$ , this can be approximated by a rectangular duct as shown and the flow equation reduces to:

$$\frac{\partial^2 u}{\partial x^2} + \frac{\partial^2 u}{\partial y^2} = \frac{1}{\mu} \frac{dp}{dz} \quad (\text{A7})$$

Where it is assumed that the pressure is a function of  $z$  alone. The boundary conditions for this element are given by the no-slip condition at the walls, i.e.  $u = 0$  at  $y = \tau$  and  $u = u_p$  at  $y = 0$ , where  $u_p$  is the (axial) piston velocity. By symmetry  $u$  is not a function of  $x$  and solving this equation gives an axial velocity profile:

$$u = \frac{1}{2\mu} \frac{dp}{dz} y^2 - \left( \frac{\tau}{2\mu} \frac{dp}{dz} + \frac{u_p}{\tau} \right) y + u_p \quad (\text{A8})$$

Now assuming a constant gas density over the element,  $\rho_m$ , the mass flow rate can be obtained by integration over the circumference of the piston:

$$\dot{m} = -\pi d_p \rho_m \tau \left( \frac{\tau^2}{12\mu} \frac{dp}{dz} - \frac{u_p}{2} \right) \quad (\text{A9})$$

Where  $d_p$  is the piston diameter.

The instantaneous pumping power,  $q\Delta p$ , can now be calculated from the volumetric flow rate,  $q$ , and integrating over the length of the piston,  $L_p$ , assuming a pressure difference  $\Delta p$ .

$$P(t) = -\pi d_p \tau \left( \frac{\tau^2}{12\mu} \frac{\Delta p}{L_p} - \frac{u_p}{2} \right) \Delta p \quad (\text{A10})$$

To obtain the usual power quoted in the literature the piston velocity is ignored (although this term is discussed below as part of the shear force on the piston), and the pressure difference is assumed sinusoidal and equal to  $p_1 \sin(\omega t)$ . The average power dissipated is then:

$$P_{\text{seal}} = \frac{\pi d_p \tau^3}{24\mu L_p} p_1^2 \quad (\text{A11})$$

In the isothermal case, where the pressure is assumed to vary in an isothermal way according to:  $p(\phi) = p_0 / (1 + \beta_v \cos \phi)$ ,

$$P_{\text{seal}} = \frac{\pi d_p \tau^3}{12\mu L_p} \left( p_b^2 - \frac{2p_0 p_b}{(1 - \beta_v^2)^{1/2}} + \frac{p_0^2}{(1 - \beta_v^2)^{3/2}} \right) \quad (\text{A12})$$

Where the buffer pressure (in the space behind the piston), is  $p_b$  and the velocity term cancels out. Since the type of compression is not fully known equation A11 will be used for the current work. Note that this power must be supplied whether or not the piston is moving, i.e. it is supplied by the PV-loop.

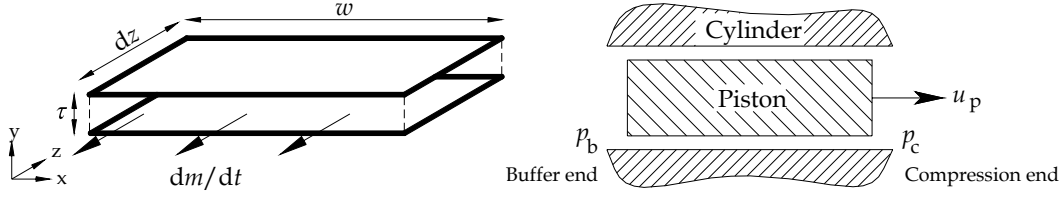


Figure 2. Geometry for calculating the mass flow in the clearance seal (not to scale).

This analysis also leads to a derivation of the piston offset pumping effect whereby the non-sinusoidal pressure variation in the compression space leads to a net pressure force to be exerted on the piston, directed into the compression space. Consider a mean density in the seal gap given by:

$$\rho_m = \frac{1}{2} \left( \frac{p}{RT} + \frac{p_b}{RT} \right) \quad (\text{A13})$$

Where  $R$  is the gas constant and  $T$  is the temperature (assumed constant). Substitution into equation A9 leads to an average mass flow rate which equals zero (in the isothermal compression case), when:

$$p_b^2 = \frac{p_0^2}{(1 - \beta_V^2)^{3/2}} \quad (\text{A14})$$

Since the average compression space pressure is given by:

$$\bar{p} = \frac{p_0}{(1 - \beta_V^2)^{1/2}} \quad (\text{A15})$$

Leading to a net pressure on the piston, towards the compression space, of:

$$p_b - \bar{p} = p_b \left[ 1 - (1 - \beta_V^2)^{1/4} \right] \quad (\text{A16})$$

I.e. the piston will be pushed forwards until the net pressure force is equalled by the restoring force of the springs.

### A.3. Shear force loss

A shear force,  $F_{\text{shear}}$ , exists between the piston and cylinder:

$$dF_{\text{shear}} = \mu \frac{du}{dy} \Big|_{y=0} dA \quad (\text{A17})$$

Evaluating this from the above velocity profile, and integrating over the surface of the piston:

$$F_{\text{shear}} = \pi D l \mu \left( \frac{\tau}{2\mu} \frac{dp}{dz} + \frac{u_p}{\tau} \right) \quad (\text{A18})$$

Where  $l$  is the length of the piston. It can be seen that there are two components to the shear force: the first is from the pressure driven gas speed and the second is because of the net gas

speed profile due to the no-slip condition applied at the seal walls. Now any power consumed by this force is not included in the PV-loop and this can be seen by considering the total force on the piston, consisting of the electrical force,  $F_e$ , the net pressure force on the ends,  $F_p$ , and the shear force on the piston circumference,  $F_s$  (ignoring any forces on any part of the piston support):

$$F = F_e - F_p - F_s \quad (\text{A19})$$

Now conservation of energy requires that the average power is zero so that:

$$\langle F_e u_p \rangle = \langle F_p u_p \rangle + \langle F_s u_p \rangle \quad (\text{A20})$$

Where  $u_p$  is the piston velocity. Now the first term is simply the total electrical input power. The second term is the PV-loop power:

$$\begin{aligned} \langle F_p u_p \rangle &= \left\langle (p - p_b) A_p \frac{dx}{dt} \right\rangle \\ &= \left\langle -p \frac{dV}{dt} \right\rangle \\ P_{\text{gas}} &= -f \int p dV \end{aligned} \quad (\text{A21})$$

Where  $A_p$  is the area of the piston end. Therefore the shear force power loss does not appear as part of the PV-loop. The power loss is given by:

$$P_{\text{shear}} = \left\langle \frac{1}{2} \pi D \tau (p - p_b) u_p \right\rangle + \frac{\pi \mu D l}{\tau} u_{p,\text{rms}}^2 \quad (\text{A22})$$

The first term is therefore equal to the power loss which was ignored in equation A10 and this shows why it was ignored: it does not form part of the PV work, although it is proportional to  $P_{\text{gas}}$ :

$$P_{\text{shear}} = \frac{2\tau}{D} P_{\text{gas}} + \frac{\pi \mu D l}{\tau} u_{p,\text{rms}}^2 \quad (\text{A23})$$

Both of these terms are typically negligible for small machines (e.g. at 55% stroke in the current machine at 5 bar with helium the loss is 0.2 mW at 55 Hz).

#### A.4. AC losses

All conductors carrying an AC current have increased resistance due to the presence of eddy currents (i.e. the AC current produces a magnetic field which induces eddy currents in the conductor, resisting the original current). For a long conductor, such as a coil, the loss can be calculated [6] and for cases where the conductor radius is less than the skin depth, such as the current machine where the coil wire radius was 0.28 mm and the skin depth for copper at 100 Hz is 6.3 mm, the ratio of the AC resistance to the DC resistance is:

$$\frac{R_{\text{ac}}}{R_{\text{dc}}} - 1 = \frac{a^4}{48\delta^4} \quad (\text{A24})$$

In the current case this factor is less than  $10^{-7}$  and the AC resistance can therefore be ignored.

### A.5. Heat exchange losses

The most well known theoretical studies of heat transfer in gas springs were conducted by Lee and by Cooke-Yarborough and Ryden. Both were based on the exact solution for a finite one-dimensional solid with a sinusoidal source-sink term. The resulting loss per cycle was calculated as:

$$W_{\text{hx}} = p_0 V_0 \frac{\pi}{2} \left( \frac{p_1}{p_0} \right)^2 \frac{\gamma - 1}{\gamma} \frac{1}{y} \left( \frac{\cosh y \sinh y - \sin y \cos y}{\cosh^2 y - \sin^2 y} \right) \quad (\text{A25})$$

With:

$$y = D_h \left( \frac{\omega}{32\alpha_0} \right)^{1/2} \quad (\text{A26})$$

Where  $\alpha_0$  is the thermal diffusivity,  $D_h$  is the hydraulic diameter,  $\gamma$  is the ratio of specific heats,  $p_0$  is the mean pressure,  $p_1$  is the pressure swing amplitude, and  $V_0$  is the mean volume. The hydraulic diameter is defined as 4 x volume/wetted area. Kornhauser and Smith compared this expression to experimental data from a similar experiment to ours, but without a clearance seal, and found it to fit reasonably well to their data.